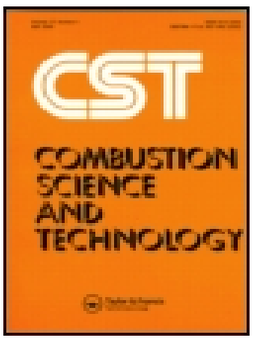

Taylor & Francis
Taylor & Francis Group

Combustion Science and Technology

ISSN: (Print) (Online) Journal homepage: https://www.tandfonline.com/loi/gcst20

Numerical Analysis on the Evolution of NH_2 in Ammonia/hydrogen Swirling Flames and Detailed Sensitivity Analysis under Elevated Conditions

Syed Mashruk, Hua Xiao, Daniel Pugh, Meng-Choung Chiong, Jon Runyon, Burak Goktepe, Anthony Giles & Agustin Valera-Medina

To cite this article: Syed Mashruk, Hua Xiao, Daniel Pugh, Meng-Choung Chiong, Jon Runyon, Burak Goktepe, Anthony Giles & Agustin Valera-Medina (2021): Numerical Analysis on the Evolution of NH_2 in Ammonia/hydrogen Swirling Flames and Detailed Sensitivity Analysis under Elevated Conditions, Combustion Science and Technology, DOI: 10.1080/00102202.2021.1990897

To link to this article: https://doi.org/10.1080/00102202.2021.1990897

Published online: 15 Oct 2021.

COMBUSTION SCIENCE AND TECHNOLOGY
https://doi.org/10.1080/00102202.2021.1990897

Taylor & Francis
Taylor & Francis Group

Numerical Analysis on the Evolution of NH_2 in Ammonia/hydrogen Swirling Flames and Detailed Sensitivity Analysis under Elevated Conditions

Syed Mashruk[a], Hua Xiao[b], Daniel Pugh[a], Meng-Choung Chiong[c], Jon Runyon[a], Burak Goktepe[a], Anthony Giles[a], and Agustin Valera-Medina[a]

[a]College of Physical Sciences and Engineering, Cardiff University, Wales, UK; [b]School of Naval Architecture and Ocean Engineering, Guangzhou Maritime University, Guangzhou, China; [c]Department of Mechanical Engineering, Faculty of Engineering, Technology & Built Environment, UCSI University, Kuala Lumpur, Malaysia

ABSTRACT

Ammonia/hydrogen blends have received some attention toward the development of new technologies focused on gas turbine combustion systems, as doping of hydrogen in ammonia enhances flame speed and stability while decreasing ignition energy. One of the challenges of these blends relies on the appropriate computational modeling of their combustion properties in combination with the complex hydrodynamics inherent to flow control techniques such as swirling flows, which are known to be the main method of flame stabilization in current gas turbines. Moreover, it is well-known that large reaction kinetic models are difficult to employ in these computational analyses, thus increasing the difficulty of obtaining reliable methods for the design of new combustors. Therefore, this research analyses a reduced chemical reaction mechanism, namely Okafor's mechanism, comparing its performance and accuracy against obtained experiments. Emission measurements and non-intrusive laser techniques (LDA) were employed to validate models running on CHEMKIN-PRO flow reactors and RANS Complex Chemistry. Once validated, the study identified the main contributors and reaction kinetics of NH_2 and NO consumption, hence evaluating the process via production rates and sensitivity analysis of various important reactions. The results depicted positive correlation between NH_2 formation and heat release, N_2, H_2O, N_2O, NH, NNH, NO, O formation, whereas NH_3, N_2H_3 and NO_2 have shown negative correlation. Statistical correlations supported these findings but unfortunately were inconclusive to the impacts of vorticity and turbulence over the production/consumption of amidogen. Sensitivity analysis has shown NH_2 radicals and atomic N to be the main contributors of NO formation in the flame zone, although most of the NO formed in the flame zone shown to be consumed at the post-flame zone due to the presence of NH_x radicals and atomic N.

ARTICLE HISTORY
Received 29 March 2021
Revised 20 September 2021
Accepted 5 October 2021

KEYWORDS
Reduced reaction mechanism; ammonia; emissions; OH/NH_x radicals

Introduction

Ammonia as an energy vector has gained increased attention across scientific and industrial communities (The Royal Society 2020; Valera-Medina et al. 2021). The role of the molecule in the decarbonization of storage technologies has potential to supplement the use of

CONTACT Syed Mashruk mashruks@cardiff.ac.uk College of Physical Sciences and Engineering, Cardiff University, Wales, UK

hydrogen with stranded renewable sources (International Energy Agency 2019). However, the implementation of ammonia technologies capable of using this vector is constrained by the improvement of their efficiency in order to reach power outputs and cost benefits similar to those of current fossil fuels (Zamfirescu and Dincer 2008). Current works have demonstrated that ammonia can be used as a relatively efficient energy storage medium (Valera-Medina et al. 2019), whilst the implementation of the technology in hybrid systems can provide economic benefits that will be competitive in the near future (Ezzat and Dincer 2018).

Progress has been made on the analysis of pure ammonia as fueling source (Kobayashi et al. 2019). Recent studies have evaluated the use of ammonia in internal combustion engines, showing that pure ammonia is difficult to burn with high unburned concentrations in the exhaust (Comotti and Frigo 2015; Lhuillier et al. 2019). Simultaneously, gas turbines have also been assessed. Better and more promising findings show that the appropriate use of advanced injection techniques can reduce unburned ammonia, thus increasing power whilst making devices more environmentally friendly with reduced NO_x emissions (Kurata et al. 2019; Pugh et al. 2019). Nevertheless, thus far, demonstration units have only provided limited power outputs (~50 kW). Since ammonia flame speed is an order of magnitude lower than hydrogen (Valera-Medina et al. 2018b), ammonia can be partially cracked to produce hydrogen prior to injection into the combustion chamber, which will enhance the energy density of ammonia blends whilst increasing reactivity, thus enabling an increase in flowrates and power outputs.

Predominantly, the use of hydrogen has been attempted in power devices fueled with ammonia (Khateeb et al. 2020; Pacheco et al. 2021; Rocha et al. 2019; Zhu et al. 2021). Further studies considered the use of ammonia/hydrogen blends at concentrations of 60/40, 70/30, 80/20 and 90/10% (vol) (Valera-Medina et al. 2018a). The results demonstrated that the 80/20 and 70/30 blends were the most stable. Since higher power outputs under much higher flowrates were conceived for the technology, the higher hydrogen content 70/30 blend was employed for additional trials. Experimental campaigns demonstrated a reduction in NO_x emissions at high equivalence ratios close to 1.20. The effect, a combination of the reduced oxygen in the primary zone and the post-combustion reaction of unburned ammonia with NO, depicted a potential blend that could be used for large-scale systems. The blend was also assessed at higher pressures, showing that the NO_x emissions are dependent on the surrounding conditions (Pugh et al. 2020). Nevertheless, the effects of intermediate combustion radicals on NO_x production/consumption are still not fully understood, leading to further work being undertaken with the support of numerical modeling (Vigueras-Zuniga et al. 2020). However, as one of the main barriers of this subject, the reaction of these highly hydrogenated mixtures is still not fully understood. Most reaction mechanisms still fail to properly predict the production of hydrogen, a by-product of the decomposition of ammonia in the primary zone of a gas turbine combustor. The models seem to be over-predicting the reactivity of hydrogen, whilst not fully resolving the cracking of ammonia into all its radicals. The problem limits the ability of using CFD models to design new combustors fueled with ammonia/hydrogen blends. Recent works (Guteša Božo et al. 2021; Pugh et al. 2020) have shown the importance of NH_2 radicals in ammonia/hydrogen flames in terms of both flame propagation and NO_x production/consumption. In that pursuit, this work has been undertaken to investigate the relationship of NH_2 radicals with other species of interest and track its change in reactivity

at slightly elevated conditions. Additionally, detailed sensitivity analysis of the species of interests has been carried out in these conditions. The results are of great interest to reaction kinetic developers as well as combustor designers working with ammonia blends.

There are many chemical kinetic models for combustion of ammonia, ammonia/hydrogen or ammonia/methane mixture fuels, e.g. Glarborg et al. (2018), Okafor et al. (2018), Mathieu and Petersen (2015), Tian et al. (2009), Konnov (2009), Lindstedt, Lockwood, and Selim (1994), Miller and Bowman (1989), Li et al. (2019b). As previously raised, for CFD modeling, reduced kinetic models are required to make computations affordable; therefore, several reduced/skeletal mechanisms have been developed employing different reduction methods as summarized by Li et al. (2019b) over the years. Ammonia mechanisms are not the exception. Most of these reduced models use different detailed kinetic mechanisms as a starting point, thus providing different results based on their independent development path. This causes conflict between users, as the results tend to vary and provide different combustion results.

Therefore, the present study initially assesses several reduced mechanisms for ammonia-hydrogen blends that have been successfully implemented in the commercial software STAR-CCM+. Chemical kinetics and emissions profiles are initially correlated using Ansys Chemkin-Pro. The most promising results serve as guidance for the selection of a reduced mechanism for its use in 3D CFD modeling. The best performing reaction mechanism, namely Okafor's (Okafor et al. 2018), was fully studied and implemented at various conditions (i.e. high temperature, elevated pressure). Furthermore, results were expanded to determine the reactivity of various reactions that have been currently conceptualized as major contributors for stability, NO formation and combustion enhancement. Therefore, the results inform modelers of the potential (or detrimental) use of each option. Further works on these models are recommended on the analyzed grounds, with suggestions for follow-up considerations.

Methodology

Experimental analysis

Initial experiments were conducted using a generic, radial/tangential swirl burner, Figure 1. An atmospheric version of this burner was analyzed in an isothermal bench. Velocity fluctuations of the flow field were measured using a Flowlite Dantec Laser Doppler Anemometer (LDA), with a dedicated Windows Software Package – BSA Flow Software, for data acquisition. The measurement matrix was designed to measure 1,000 points with 1 mm step on the horizontal axis by 1 mm step on the vertical plane. In each case, the seeding particles, i.e. aluminum oxide, were kept at 10,000 counts, which was far above the minimum accuracy level of 2,000 (Dantec Dynamics 2017). An intrusive Constant Temperature Anemometer CTA, with Stream Ware, a Windows-based software, was used to measure the flow velocity profiles to validate the measurement from the LDA, which provided a deviation between techniques of 3.2%.

The tests were conducted in a High Pressure Optical Combustor (HPOC), Figure 1, which enabled to account for non-adiabatic conditions in the system, which are known to produce higher NO_x and lower NH_3 consequence of higher reactivity (Manna et al. 2019; Vigueras-Zuniga et al. 2020). The experimental system, detailed elsewhere (Pugh et al. 2019; Valera-Medina 2020), established the boundary conditions of the CFD model, Table 1. At

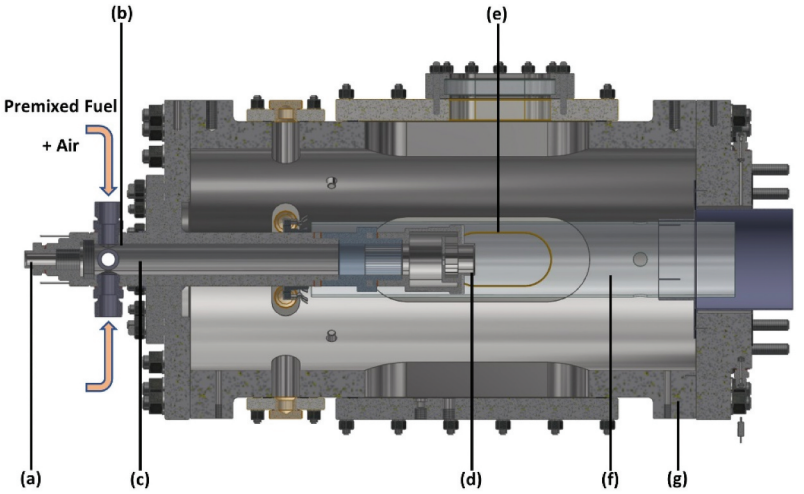

Figure 1. Experimental rig for combustion tests (a) instrumentation and pilot injection lance, (b) inlet plenum, (c) premixed chamber, (d) radial-tangential swirler, (e) quartz window, (f) quartz burner confinement tube, and (g) high-pressure optical casing.

Table 1. Experimental and numerical boundary conditions.

Experimental		Numerical	
Parameter	Value	Parameter	Value
Blend	70–30 NH_3-H_2 (vol%)	Quartz Temperature	1560, 1585, 1590 K
Mixing	Fully pre-mixed	Burner section	Symmetry (120°)
Equivalence Ratio (Φ)	1.2	Swirler walls	Adiabatic
Inlet Velocity	2.5 m/s	Ignition Temperature	3000 K
Inlet Temperature	323 (T1), 411 (T2), 499 (T3) K	Turbulence	10%
Inlet Pressure	0.11 (P1), 0.14 (P2), 0.17 (P3) MPa	Walls	No-slip
Outlet Pressure	0.10, 0.13, 0.16 MPa	Method	Segregated Flow
Swirl	0.8	Mechanisms	Okafor/Li/Glarborg

elevated conditions, temperature and pressure were increased in such a way so that constant T/P ratio is maintained, retaining quasi-steady nozzle outlet velocities and combustor residence time for same Φ (Pugh et al. 2020). The experimental results (Pugh et al. 2020) were also used for validation purposes.

Combustor exhaust gas emissions were sampled downstream of the quartz confinement using a 9-hole equal-area probe, water-conditioned with a heat exchanger to regulate sample temperature (433 K) following specifications in ISO-11042 (British Standard 1996). Nitric oxide concentrations were quantified using heated vacuum chemiluminescence (Signal 4000VM). Unburned NH_3 measurements were obtained by redirecting sample through an NO converter (Signal 410) to measure unreacted concentrations (80% conversion efficiency). All NH_3 and NO concentrations were measured hot/wet and normalized to equivalent dry conditions (ISO-11042). Dry O_2 concentrations were quantified using a paramagnetic analyzer (Signal 9000MGA) and used to subsequently normalize NO to equivalent 15% O_2 (ISO-11042). After changing experimental conditions, burner temperatures, pressures, flows and emissions were monitored and, once stable, held for

a minimum of 60 samples to be taken. Systematic uncertainties comprising analyzer specification, linearization and span gas certification were combined with any fluctuations in measurement to give the total uncertainty ~5%.

Chemical kinetic modeling

Analysis was performed using CHEMKIN-PRO and at the experimental inlet conditions. Table 1 details the boundary conditions used for chemical kinetic modeling and CFD modeling detailed in the next section. The PREMIX code (Kee et al. 1985) and the EQUILIBRIUM tool (Gordon and McBride 1976) were used to calculate the global properties of a simplified laminar flame. An adaptive grid of 1000 points was employed with mixture-averaged transport properties and trace species approximation. The mechanisms from Okafor et al. (2018), Li et al. (2019b) and Glarborg et al. (2018) were employed and compared with both experimental and numerical results. The objective was to better understand the discrepancy between models and address the most sensitive reactions to the production of important species such as NH, NH_2 and OH. Okafor's (Okafor et al. 2018) mechanism was chosen for sensitivity analysis on the basis of further validations explained below.

A chemical reactor network (CRN), previously developed elsewhere (Guteša Božo et al. 2021; Mashruk, Xiao, Valera-Medina 2020; Mashruk 2020), was employed to model the combustion zone, Figure 2. Mixing zones, flame zones, central recirculation zone (CRZ) and external recirculation zone (ERZ) were modeled by individual perfectly stirred reactors (PSR), and the volume and residence time for each PSR were obtained from previous RANS CFD analysis (Vigueras-Zuniga et al. 2020). The recirculation strength was determined by previous experimental campaigns that employed comparable burners (Mashruk 2020; Valera-Medina, Syred, Bowen 2013), as well as from the LDA measurements undertaken in this study. The calibration of the model for determination of residence time and heat loss in the rich flame zone was achieved in accordance to previous experiments (Syed Mashruk 2020; Valera-Medina et al. 2019; Valera-Medina et al., 2018c). The post-flame zone was modeled by a plug flow reactor (PFR) with one dimensional length of 30 cm.

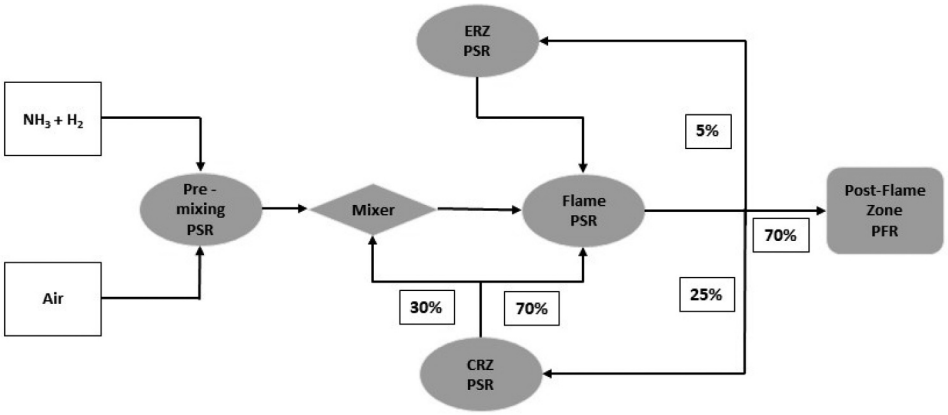

Figure 2. Chemical reactor network (CRN).

Numerical modeling

The software Star-CCM+ v19.3 was employed to conduct CFD analysis using Okafor's reduced reaction mechanism, which performed the best during the validation campaign, detailed below. The analysis was conducted using RANS k-w SST modeling that is known to provide good average results for tangential swirling flows (Baej et al. 2014; Eriksson 2007). Second-order discretization was employed for convection of segregated flows, whilst curvature correction was applied to the turbulence model. For the resolution of combustion, reacting species transport with Complex Chemistry was employed in combination with the Turbulent Flame Speed Closure model. The model employs Zimont's Turbulent Flame Speed approach, which includes wall effects for quenching the flame near these regions with unburnt thermal diffusivities estimated using a power law. Simultaneously, clustering methods were employed to reduce the computational expense of Complex Chemistry calculations (Siemens 2019).

Initial analysis was performed to compare the hydrodynamics within the system, with special emphasis on velocity profiles, coherent structures and flame features (i.e. angle, diameter, etc.). Posteriorly, combustion analysis was validated using emission results from previous campaigns (Pugh et al. 2020). For CFD resolution, a numerical mesh consisting of 3.4 million cells was used for the calculations, Figure 3. The mesh represents only one-third of the entire section of the burner. Periodicity was established in all the side frontiers of the mesh in order to simulate the entire flow. The mesh was improved using Local Mesh Refinement in the downstream zone of the burner, just passed the nozzle where CRZ and shearing flow are formed. Preliminary characterization was conducted for a mesh independency analysis. Meshes with ~1.5, 3.4 and 7.5 million cells were also compared, with the intermediate cell providing similar results to the finest case and 2/3s of the time for resolution. Residual values ranged from 10^{-4} to 10^{-9}.

Further numerical modeling was conducted to determine the impact of different species on NH_2 production rates. Eight planes, shown in Figure 3, were compared with spacing of 0.10D, D being the diameter of the burner outlet. Results were then evaluated at various

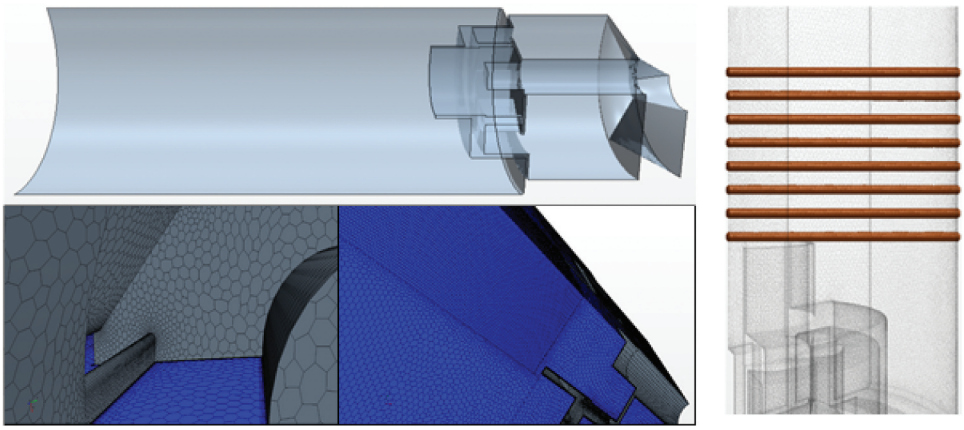

Figure 3. Mesh used for modeling. Top) Surface of tangential swirl burner; Bottom) volumetric mesh; Right) measurement positions. The mesh has been refined at the center where CRZ and shearing flow are formed.

pressures and inlet temperatures to determine the impact of these variables on the production/consumption and reactivity of NH_2. All simulations were conducted using a blend of 70–30 (vol%) ammonia-hydrogen as measured in previous experimental campaigns (Pugh et al. 2019; Valera-Medina et al. 2017; Valera-Medina 2020).

Results

CFD validation at isothermal flow conditions

Initial calculations were compared with isothermal experiments in order to determine that the hydrodynamics of the systems were in accord with those of the numerical model. The results provided in Figure 4 show good agreement for the velocities and formation of coherent structures across the burner. A well-formed CRZ appears in the middle of the system, with a shearing flow characteristic of these flows and at similar overall attributes as those recorded in previous experiments (Runyon et al. 2015, 2018; Valera-Medina et al. 2017). It is believed that discrepancies in the length of the central recirculation zone for the intermediate planes (i.e., located at 33 and 43 mm) are caused by the turbulence model employed (RANS) that does not account for complex structures such as the precessing vortex core that squeezes the coherent structure. However, the result evidence good accuracy between model and experiments with same trends, peak values and shearing flow location. Therefore, having confidence on the hydrodynamics of the flow, the study progressed into the use of combustion for evaluation of a reduced mechanism.

CFD validation under combustion conditions

Numerical simulations were carried out based on the experimental conditions, Table 1, reported by Pugh et al. (Pugh et al. 2020). Initial analysis was conducted using the CRN, Figure 2, to determine the mechanism that would be employed for 3D CFD simulations. Three mechanisms, namely Okafor et al. (2018), Li et al. (2019a) and Glarborg et al. (2018), were compared, Figure 5. The seemingly increasing NO production with increasing pressure can be attributed to increasing inlet temperature (Pugh et al. 2019, 2020). As can be seen, these mechanisms either overpredict (Li), underpredict (Okafor) or do not correlate (Glarborg) the experimental NO emissions obtained for the blend and operational conditions attempted in this work. Most mechanisms overpredict the production of OH radicals

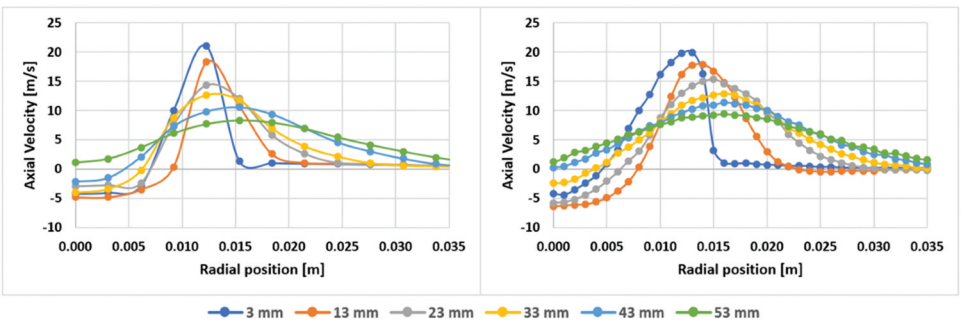

Figure 4. Isothermal results. Left) numerical model; right) LDA experiments.

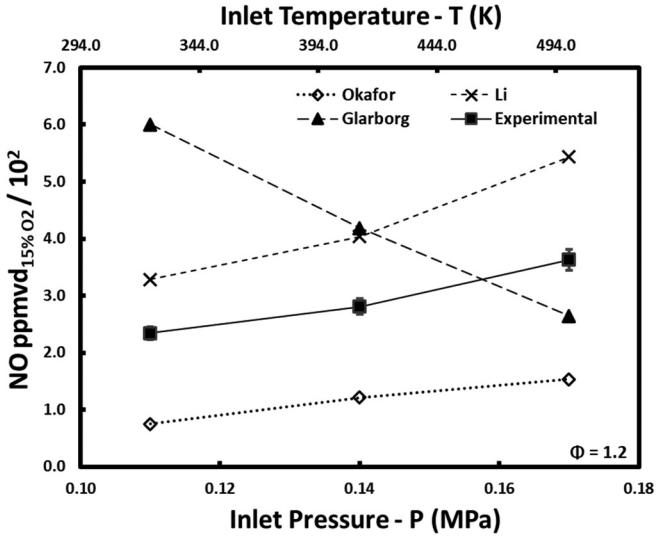

Figure 5. Comparison between experimental results and mechanisms predictions.

(Mashruk, Xiao, Valera-Medina 2020) which are directly correlated to NO/ammonia recombination processes. Although these are still points for improvement in such mechanisms (Elishav et al. 2020), the order of magnitude of the NO emissions between experiments and numerical simulations (Li and Okafor) is similar. Even though Li's predictions were closer to experimental results, Okafor's mechanism was employed for CFD resolution since the trends are the same, previous work has shown good correlations for ammonia flames (Kobayashi et al. 2018), the mechanism is a reduced version of Tian's mechanism (Tian et al. 2009) whose validation has also been widely confirmed (Elishav et al. 2020), and the low number of species (27) and reactions (130) make it a model with low computational costs, a critical parameter for the solution of these multi-physical processes.

3D CFD analysis using Okafor's mechanism was compared with experimental data, Figure 6. NO emissions are in accord with those obtained using the CRN, following similar trends and values. Interestingly, unburned ammonia concentrations are properly resolved at elevated pressure and inlet temperatures. Unfortunately, correlation under atmospheric conditions is poor with a 3-fold discrepancy between values. This is a problem that is well-known for the use of current mechanisms. For the case of Okafor's model, although it has shown very good resolution in other experimental campaigns, the impact of different hydrodynamics and reaction ratios affect the final results, thus still requiring further improvements out of the scope of this work. Recently, Colson et al. (2020) showed how the resolution of existing mechanisms is still inaccurate for certain premixed ammonia-based blends. Thus, only the points T2/P2 and T3/P3 (refer to Table 1) were used for CFD analysis. However, all the conditions (T1/P1, T2/P2, T3/P3) were considered for sensitivity and ROP analysis in Chemkin-Pro platform with Okafor's reduced mechanism (Okafor et al. 2018) as the initial results displayed the similar experimental trend, Figure 5. It is again emphasized the crucial need to keep improving the resolution of these and other chemical kinetic mechanisms for better correlations.

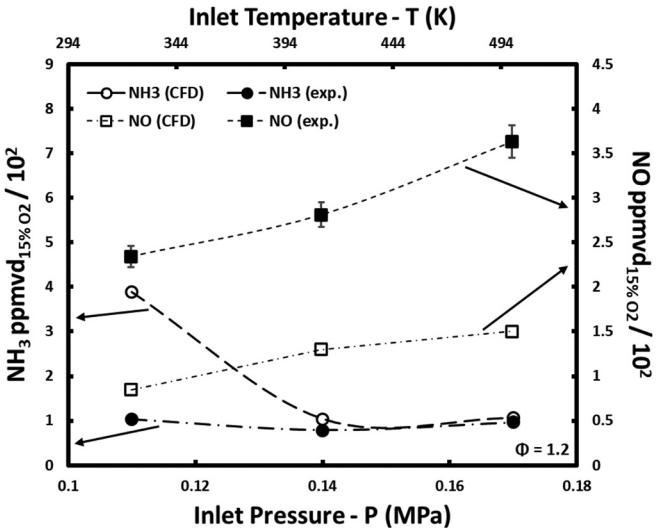

Figure 6. Correlation between experiments and 3D-CFD simulations, NO and NH_3 emissions.

NH_2 correlation with pools of radicals and energy

As depicted previously, one of the most important radicals in ammonia flames is NH_2, which is known to drive many of the processes in these flames. However, to have a deeper understanding of the effect of NH_2 at different conditions, the numerical analysis focused on resolving this species and its impacts on other important parameters across the flame. The discussion is conducted with an intermediate inlet pressure (P2) and intermediate inlet temperature (T2), Table 1, for further comparison with T3/P3 condition later on.

Preliminary results show the large production of NH_2 at the flame front/shearing flow, Figures 7 and 8 . This is the region of highest temperature at the flame zone, increasing the enthalpy in the amidogen (NH_2) molecules, Figure 9, with higher heat release, Figure 10. These results are in line with experimental results obtained by others (Pugh et al. 2020), where NH_2 seems to be formed closer to the upper part of the flame. NH_2 is the main fuel-derived radical, and its presence is an indication of where NH_3 is actually consumed. The conversion of NH_3 to NH_2 is further analyzed in Section 3.5. NH_2 radicals participate in further DeNOxing (Coutant, Merryman, Levy 1982; Miller et al. 1985; Prada and Miller 1998) purposes via $NH_2 + NO \rightarrow H_2O + N_2$. Due to the higher reactivity of NH_2 compared to ammonia and other species (i.e. NO), the signature of this molecule remains a high contributor to the reaction as depicted by others (Hayakawa et al. 2015) and addressed next, shifting the wavelength to the orange spectrum representative of NH_2 combustion (between 543 and 665 nm (Pearse and Gaydon 1976)), an observed trend discussed elsewhere (Valera-Medina et al. 2019).

Major radicals were extracted at different axial locations, as shown in Figure 3. The results, Figure 11, denote some of the impacts of reactivity and interaction between species along the radial distance. The data in the figure has been normalized for the ease of

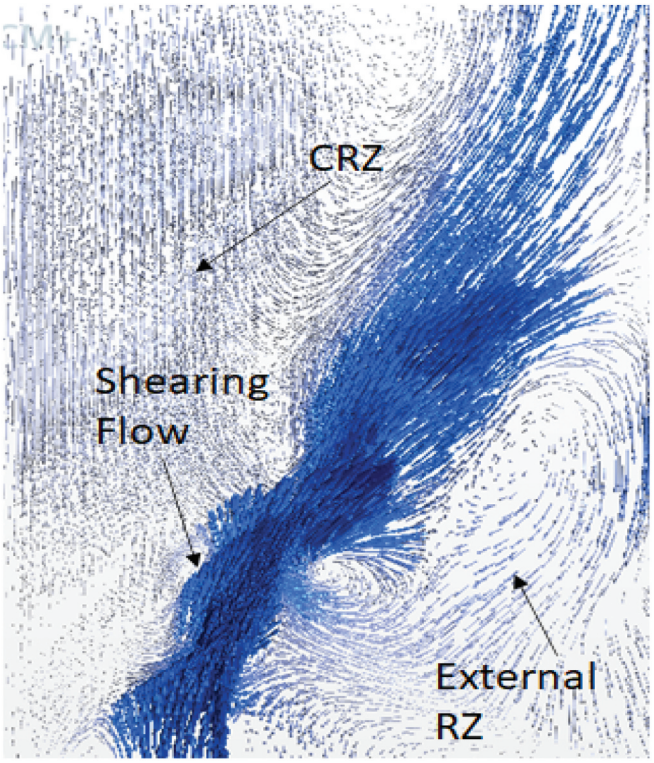

Figure 7. Coherent structures within the field.

comparison at one constant axial distance (0.001 m). The selected normalization method was based on using the maximum and minimum values within the obtained data from the simulation,

$$x_{normalized} = \frac{x - x_{min}}{x_{max} - x_{min}}$$

x being the parameter in consideration. Normalized images at all the other locations, Figure 3, are given in supplementary material, Figs. S01–S07. Figures containing the raw data with all eight axial distances have been made available in the supplementary material, Figs. S08–S09.

It is clear that there are many peaks that are in accord with the highest NH_2 production zones. For example, the highest chemical heat release denotes clear NH_2 production peaks. Similarly, N_2 shows correlated peaks with minor delay located within the central recirculation zone, consequence of the reaction of NH_2 with nitric oxide (NO) to produce the nitrogen molecule, a trend that repeats with H_2O due to the reaction NH_2+ NO→N_2+ H_2 O. Similarly, NO and N_2O show clear, positive trends with the production rates of amidogen, with all peaks slightly displaced within the central recirculation zone. However, due to the large data, there are many relations within these results that need to be statistically

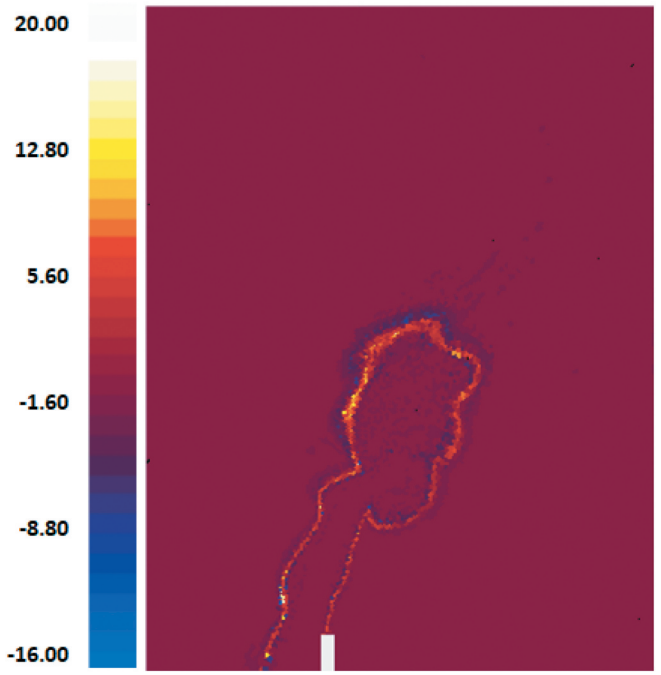

Figure 8. Rate of production of NH_2, T2/P2 conditions. Units [kg/m^{3}s].

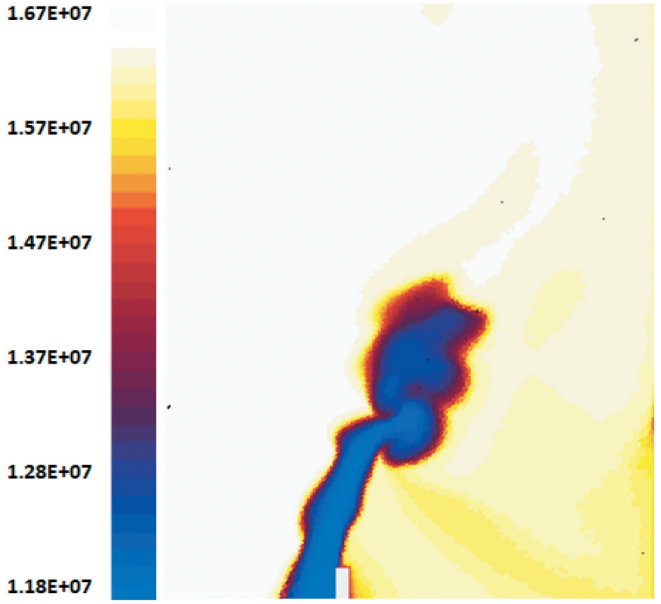

Figure 9. Enthalpy of NH_2, T2/P2 conditions. Units [kg/m^{3}s].

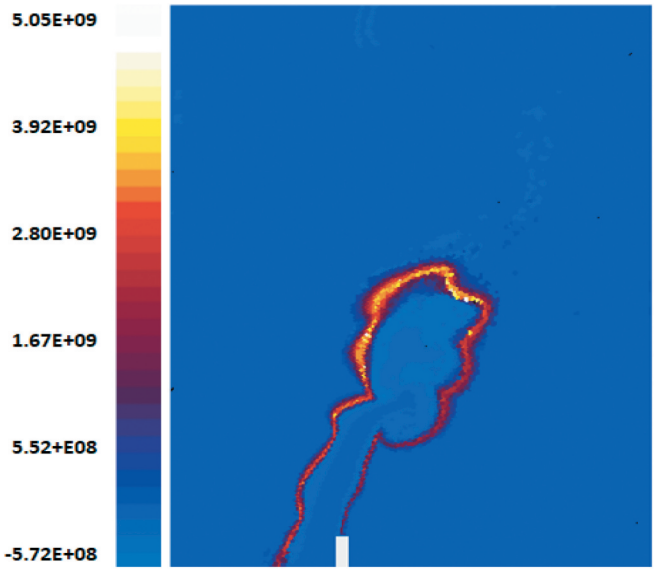

Figure 10. Heat release rate, T2/P2 conditions. Units [J/m^{3}s].

correlated to NH_2 production, as some hidden parameters escape visual correlation across the studied planes. Therefore, statistical correlations have been established using the following approach:

$$Corr(Y,Z) = \frac{Covariance(Y,Z)}{\sigma_Y \sigma_Z}$$

Being Y the NH_2 variable, Z another variable form the available set of parameters, *Corr(Y,Z)* is the statistical correlation between variables Y and Z, σ_Y and σ_Z the standard deviations of variables Y and Z, respectively. The results, Figure 12, show the correlation between parameters and NH_2 across the flame in the studied positions, Figure 3. Similarly, these correlations were plotted using a Principal Component Analysis (PCA), Figure 13.

Principal component analysis (PCA) is a technique for reducing the dimensionality of such datasets, increasing interpretability but at the same time minimizing information loss. It does so by creating new uncorrelated variables that successively maximize variance (Jolliffe and Cadima 2016). PCA is defined as an orthogonal linear transformation that transforms the data to a new coordinate system such that the greatest variance by some scalar projection of the data comes to lie on the first coordinate (called the first principal component), the second greatest variance on the second coordinate, and so on (Jolliffe 2002).

Up to 24 principal components were recognized using the software Analyze-it®, Figure 13. The first two components contribute to 59.3% of analysis, with positive correlations shown with angles below 90°, no correlation at 90°, and negative clear correlations between species at angles close to 180°. As visually depicted from previous results, Figures 11 and 12 , Chemical heat, H_2O, N_2, NO, N_2O and NNH show clear positive correlations with NH_2 across the flame. There are also other clear negative correlations such as NH_3. However, other species with week/no correlations are also evident with this analysis, for example,

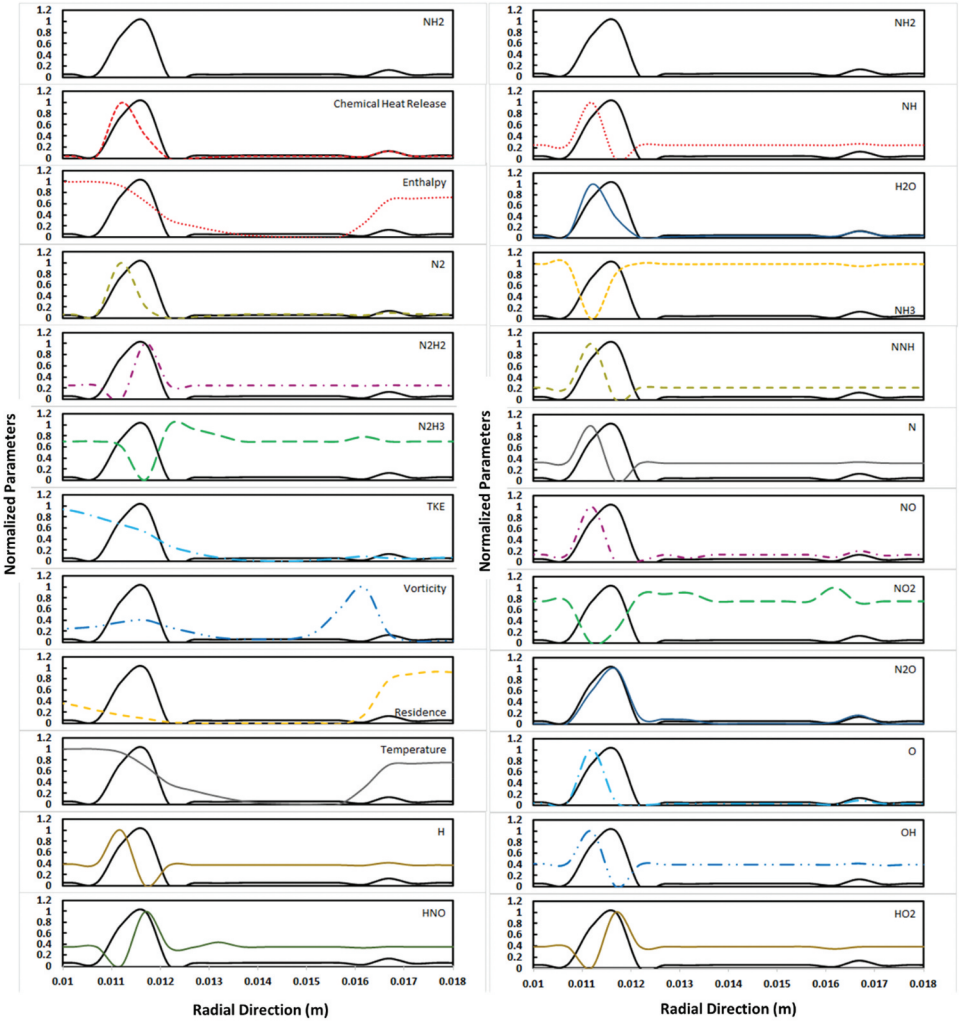

Figure 11. Comparison between normalized production rates of NH_2 and other species and parameters at 0.001 m from the burner exit.

O and NH. This is an expected behavior consequence of the high reactivity of NH_2 and the high temperatures in this region, leading to the production of species such as O and NH that impact on the production of nitrogen oxides via HNO, which interestingly does not show an evident correlation across all the layers of the flame. Furthermore, contrary to what would be expected, NO_2 is mostly consumed within these peaks, likely due to the high concentration of NH_2 and high temperatures, leading to decomposition and recombination of nitrous oxides, trend that is observable in these results.

Molecules such as O and NH also show peaks correlated to the highest point of production of NH_2, Figure 11, as would be expected due to the increased reactivity of oxygen and the formation of OH that interacts with ammonia for the decomposition of the latter to form NH_2. However, other radicals such as NNH and N_2H_2 also denote an increase in production with NH_2. Whilst NNH is known to be a molecule that is of great importance

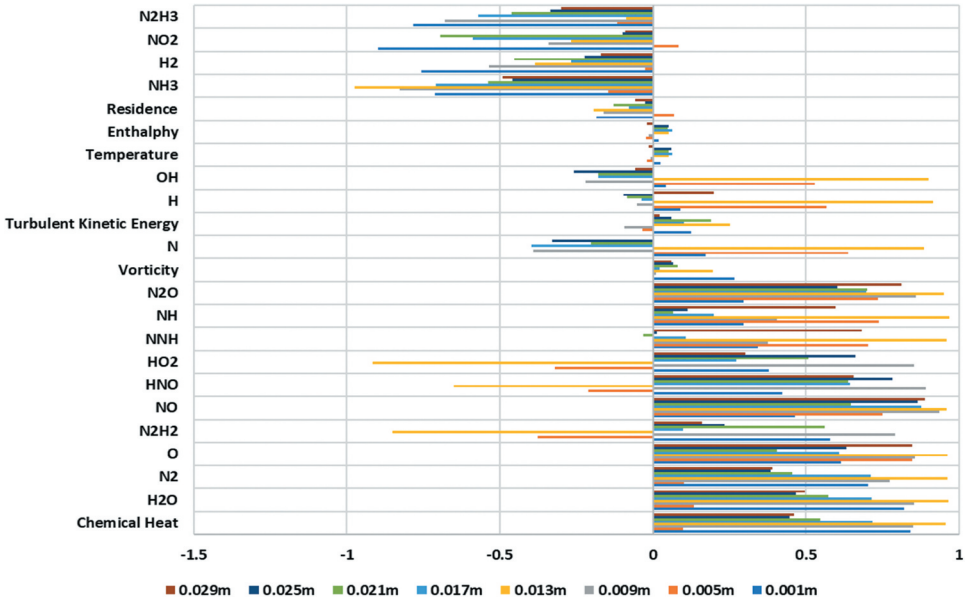

Figure 12. Correlations between NH_2 and the rest of species and parameters at different locations according to Figure 3.

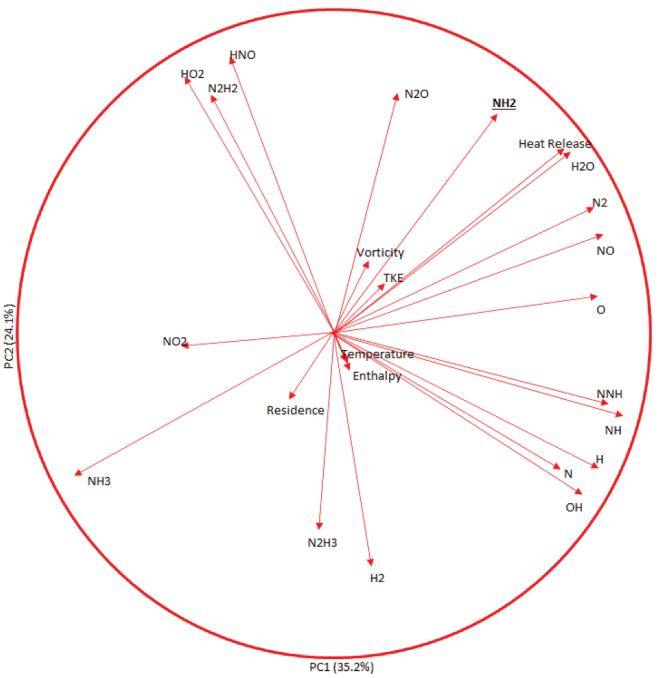

Figure 13. Bipolar multivariable analysis. Most correlations are depicted as described in Table 2.

Table 2. Correlations to NH_2 production/consumption of species and other parameters.

Parameters/Species	Observed correlation with NH_2
Enthalpy	No clear correlation.
Heat Release	Shows a clear, high, positive correlation. Heat release peak is slightly delayed near the burner exit but coincide with the NH_2 formation at the higher axial positions.
N_2	Slightly delayed within the CRZ at the burner exit while coincide at the center of the flame and deviate again at higher axial positions, but it presents a clear, positive correlation.
N_2H_2	No clear correlation.
N_2H_3	Shows in all NH_2 peaks negative valleys of different sizes. Clear negative correlation.
TKE	No clear correlation.
Vorticity	Positive, weak correlation.
Temperature	No correlation.
H	Peaks and valleys, no clear correlation.
H_2O	Shows a clear, high, positive correlation.
HNO	Peaks and valleys, complex correlation.
HO_2	Peaks and valleys, complex correlation.
N	Not clear correlation.
N_2O	Shows a clear, high, positive correlation.
NH	Slightly delayed correlation within the CRZ at the burner exit while coincide at the center of the flame and deviate again at higher axial positions, with positive correlation.
NH_3	Shows a clear, negative correlation.
NNH	Slightly delayed correlation within the CRZ at the burner exit while coincide at the center of the flame and deviate again at higher axial positions, with positive correlation.
NO	Shows a clear, high, positive correlation. Slightly delayed peak at the burner exit while coinciding at the center of the flame.
NO_2	Shows a clear, negative correlation.
O	Shows a clear, positive correlation.
OH	Peaks and valleys. No clear correlation.

in the consumption of N and NO (Klippenstein et al. 2011), its production under these conditions is 2 orders of magnitude lower than the production of NO, thus slightly contributing to the consumption of nitric oxides in this region. Moreover, molecules such

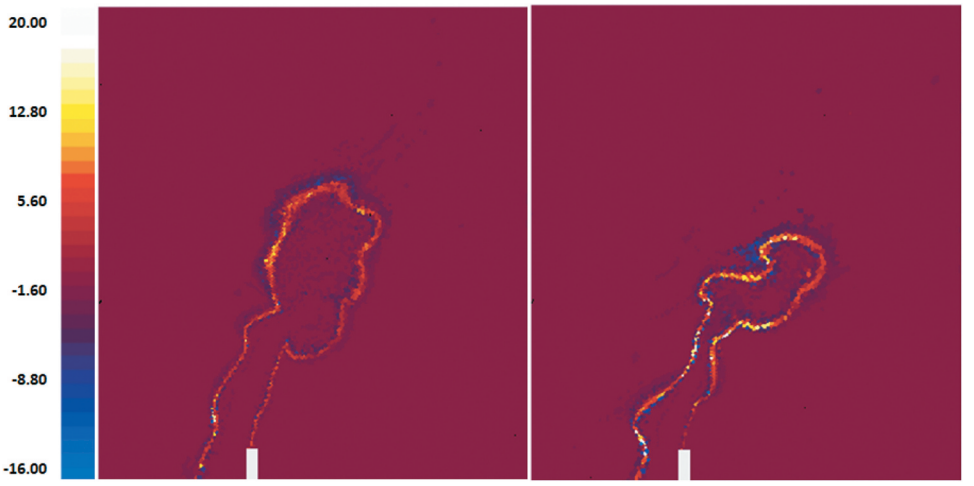

Figure 14. Production rate of NH_2. (a) T2/P2, and (b) T3/P3 conditions. Units [kg/m3s].

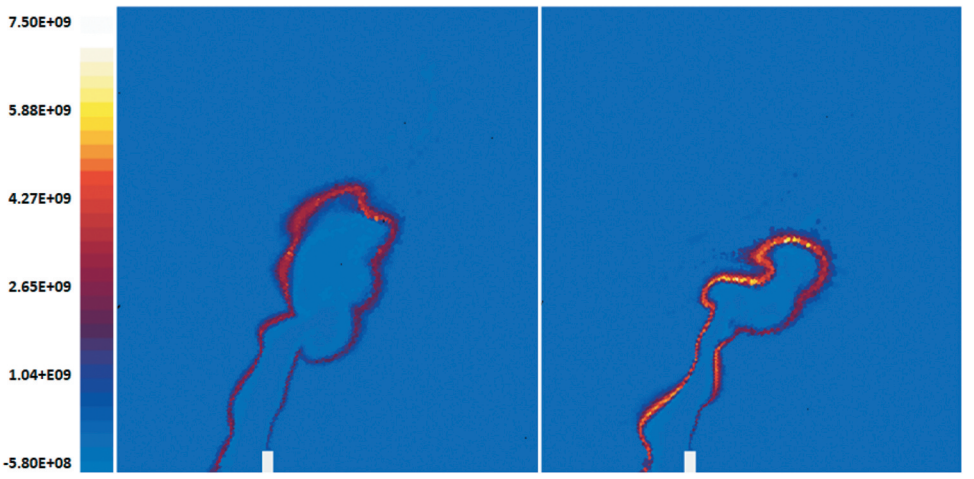

Figure 15. Heat release rate. (a) T2/P2, and (b) T3/P3. Units [J/m^3s].

as N_2H_3 have received less attention. It must be emphasized that the latter shows a negative correlation to the production peaks of amidogen as N_2H_3 is formed directly or indirectly from NH_2 recombination reactions, thus acting as a species whose consumption greatly impacts the formation of NH_2. Due to the high reactivity of NH_2, the correlation with residence time, Turbulent Kinetic Energy (TKE) and vorticity, which are orders of magnitude greater than amidogen's chemical reaction rate, are not strong. For instance, vorticity shows always positive, weak correlation, whilst turbulence does not show an evident trend. Similarly, temperature and enthalpy do not have a clear correlation to NH_2. Vorticity is the only hydrodynamic value with a considerable correlation across low to medium layers, a parameter that will be further explored at the elevated conditions to elucidate any real correlation to the production of amidogen.

Further analyses were conducted on NO reduction. Different to the peaks of NH_2, the consumption of nitric oxides mostly correlates to the consumption of NNH, O, NH_2 and a slight increase in residence time, Figures 11–13. Furthermore, N does not appear to have a clear correlation with NH_2. These results are in accord with other studies (Glarborg et al. 2018; Klippenstein et al. 2011; Skreiberg, Kilpinen, Glarborg 2004) that raise the importance in the balance of the formation of pools of radicals and temperature profiles for the reduction of NO concentration. However, as depicted here, the use of flames with limited control in species recombination and residence time control can be detrimental to the formation of pollutants, thus requiring more strategic injection philosophies. A summary of the observed trends is shown in Table 2.

Impact due to change in inlet pressure and temperature

Results denote how at different inlet temperatures and pressures a critical change in NH_2 reactivity and chemical heat release occurs in Figures 14 and 15 . Furthermore, the size of the flame has also contracted at higher pressure with a thinner, more active reaction layer for the production of NH_2. Interestingly, NH_2 shows not only more production but also higher consumption ratios at elevated conditions, thus leading to higher NO emissions in the flame zone, which can be attributed to increased inlet temperature (Pugh et al. 2020). This has been demonstrated experimentally elsewhere (Valera-Medina et al. 2019). Furthermore, recent results obtained by Pugh et al. (2020) denote the considerable increase in NH_2^* chemiluminescence at higher inlet temperature and pressure conditions, thus being in accord with the results here presented, thus indicating proportionality between ground state NH_2 and electronical excited state NH_2^*.

This increase in NO emissions is also in accord with the results observed in section 3.3, where the high peaks of NH_2 specify the locations where the reaction of amidogen with combined pools of OH, O and H deliver high NH concentrations that interact with OH to form HNO, precluding the production of NO. However, different to those cases at lower temperature and pressure, unburned ammonia, and larger unconsumed pools of NH_2 located in colder recirculation zones keep acting further downstream the flame zone in post-flame regions, mitigating the overall production of NO emissions at the outlet of the combustion zone. Detailed sensitivity analysis at Section 3.5 shows how the increase in pressure accompanied by higher inlet temperatures not only promotes NO at the flame but also ensures that unreacted NH_x can recombine with surrounding NO_x molecules to mitigate pollutants.

Vorticity and its impacts on the production of NH_2 were also assessed to determine whether the correlation between these parameters exists or not, Figure 12. Vorticity and vortical structures were extracted from the flow field, Figure 16. The Q-criterion was used to extract the vortical structures (Jeong and Hussain 1995),

$$Q = \frac{1}{2}\left(\left\|\mathbf{W}^2\right\| - \left\|\mathbf{S}^2\right\|\right)$$

Where **W** the vorticity tensor and **S** the rate-of-strain tensor.

Figure 16a denotes how vorticity is highly localized close to the dumping plane and through the boundaries of the flame and recirculation zone, an expected result. However, Figure 16b,c, shows that the production of NH_2 (weak positive correlation, Figures 12 and 13) does not appears consistent through the boundaries of the vortical structures, with only

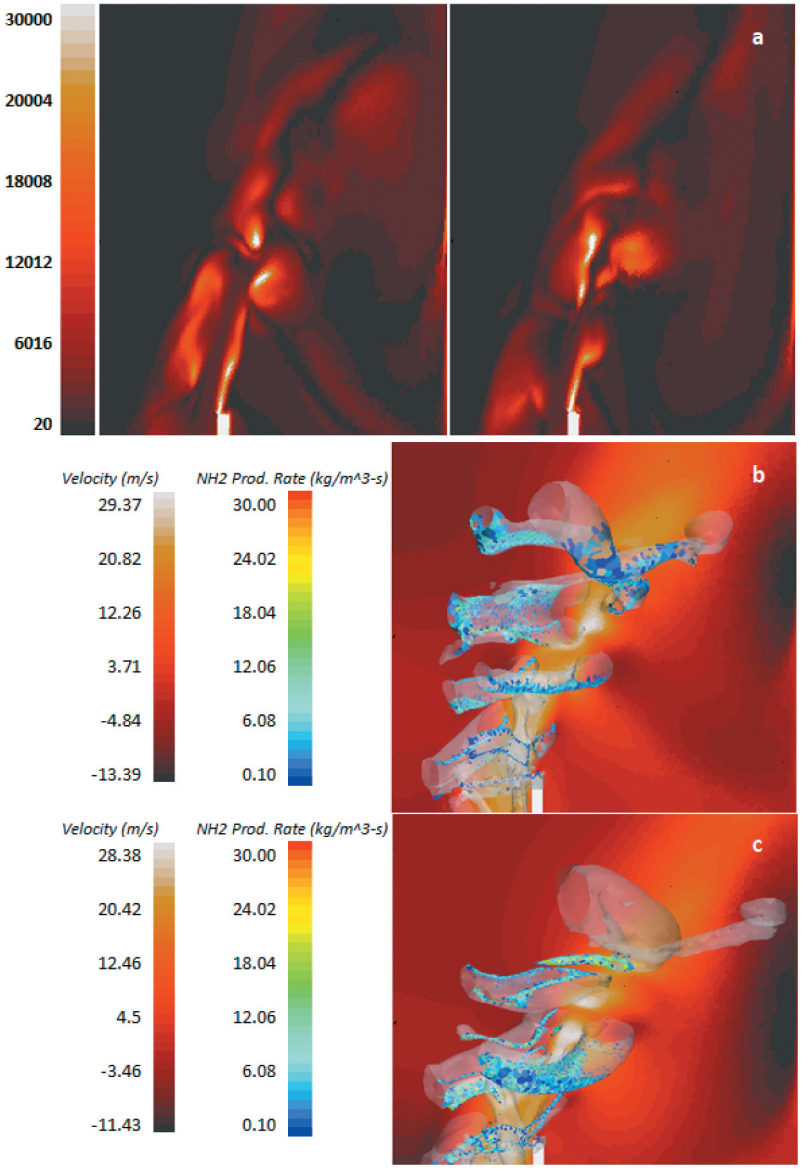

Figure 16. (a) Vorticity [1/s] in T2/P2 (left) and T3/P3 (right); (b) T2/P2 and (c) T3/P3 superimposed NH_2 production over vortices identified at Q = 5e+6 over axial velocity background.

the upper structures showing some decent production points. Although it was expected that the vortical structures would play a more critical role in the production/recombination of NH_2 due to enhanced residence and mixing time, the current results show the opposite. The effect seems to occur mainly in the area facing the inner core of the recirculation zone and the flame. Nevertheless, it must be emphasized that the resolution of these vortical structures is not as rigorous as with other turbulence models (i.e. LES), hence leaving this subject inconclusive and as a potential for further research.

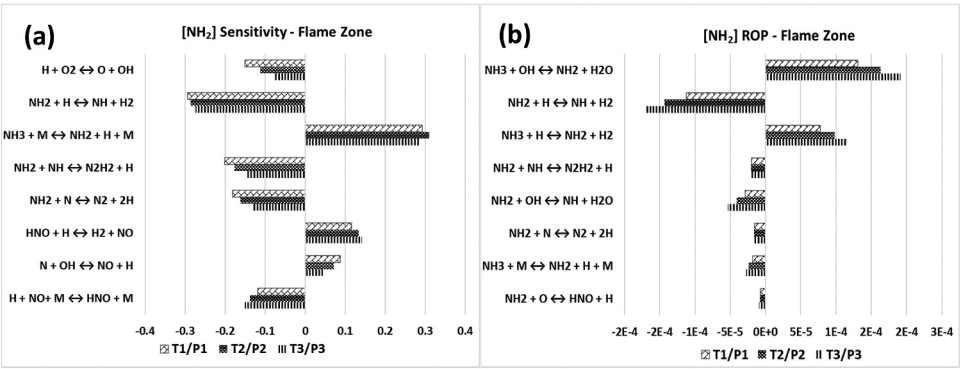

Figure 17. (a) Normalized sensitivity coefficients, and (b) absolute ROP of $[NH_2]$ at the flame zone.

Sensitivity analysis

Further analysis, Figures 17–24, show the previous trends and those occurring in the post-combustion zone.

For example, Figure 17a,b show the calculated normalized sensitivity and absolute rates of production (ROP) of NH_2 at the flame zone, respectively. The reactions responsible for overall NH_2 production and consumptions have the lowest ROP at T1/P1 conditions and the highest ROP at T3/P3. The elevated conditions increase the reaction rate of the reactions under consideration, Figure 17b. However and interestingly, in terms of sensitivity coefficients, most of the reactions show higher sensitivity for atmospheric conditions than the elevated conditions, thereby it can be concluded that even though elevated conditions have higher ROP at the flame zone, these reactions have larger effect on overall NH_2 at atmospheric conditions. NH_3 reacts with OH and H radicals to produce NH_2 radicals, which in turn reacts with OH and H radicals again to produce NH radicals, prompting the reaction $H + O_2 \leftrightarrow O + OH$ (R1) to have overall negative sensitivity for NH_2 at the flame zone, Figure 17a.

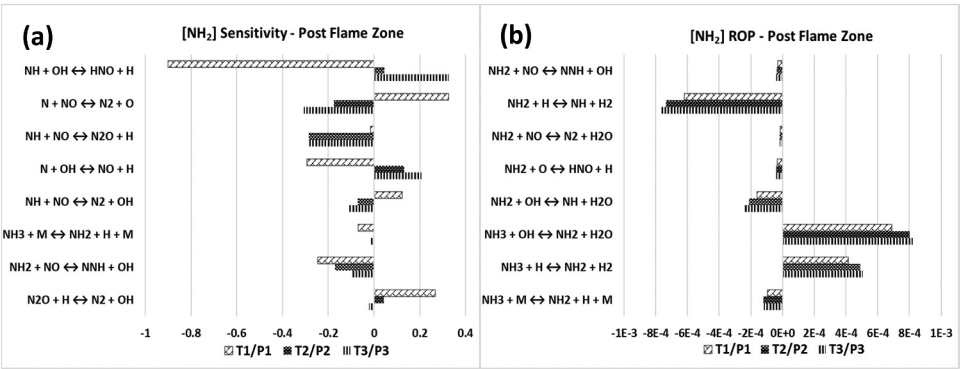

Figure 18. (a) Normalized sensitivity coefficients, and (b) absolute ROP of $[NH_2]$ at the post flame zone.

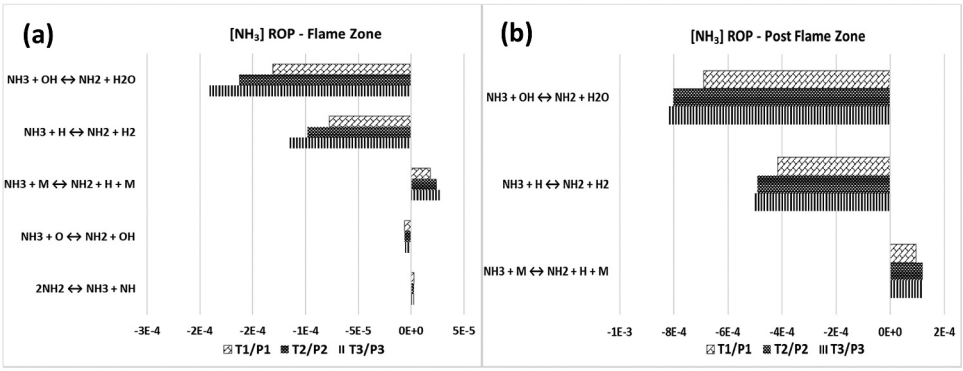

Figure 19. Absolute ROP of [NH_3] at (a) the flame zone and (b) the post-flame zone.

As the fuel was burnt under rich conditions at the flame zone, some of the unburnt NH_3 escapes rich flame zones and reacts with available radicals in the post-flame zone to convert into $NH_3 \rightarrow NH_2 \rightarrow NH$. At the same time, some of the NH_2 radicals convert back to NH_3 through the third body reaction $NH_3 + M \leftrightarrow NH_2 + H + M$ (R2), operating at reverse direction. Interestingly, the reactions $NH + OH \leftrightarrow HNO + H$ (R3) and $N + OH \leftrightarrow NO + H$ (R4) display negative sensitivity for NH_2 at atmospheric condition but positive sensitivity for elevated conditions, whereas the reactions $N + NO \leftrightarrow N_2 + O$ (R5) and $NH + NO \leftrightarrow N_2 + OH$ (R6) show positive sensitivity for NH_2 at atmospheric condition but negative sensitivity for elevated conditions at the post-flame zone, Figure 18a. Reactions R3 and R4 operate at forward direction at T1/P1 condition, opposed to the elevated conditions, thus restricting the availability of OH radicals for NH_3 conversion to NH_2, resulting in negative sensitivity. Reaction R5 operates at forward direction for all the conditions considered here but has significantly lower ROP at atmospheric condition than the elevated conditions. This low ROP of reaction R5 can be attributed to the forward/backward operation of reaction R4, thus limiting the availability of atomic N at the atmospheric condition for R5 to occur, which in turn limit the conversion of NH_2 to HNO by reacting with O radicals. Reaction R6 operates at

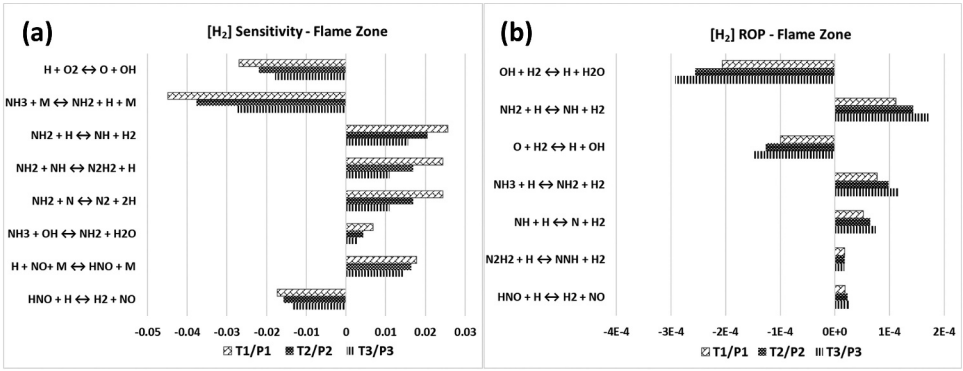

Figure 20. (a) Normalized sensitivity coefficients, and (b) absolute ROP of [H_2] at the flame zone.

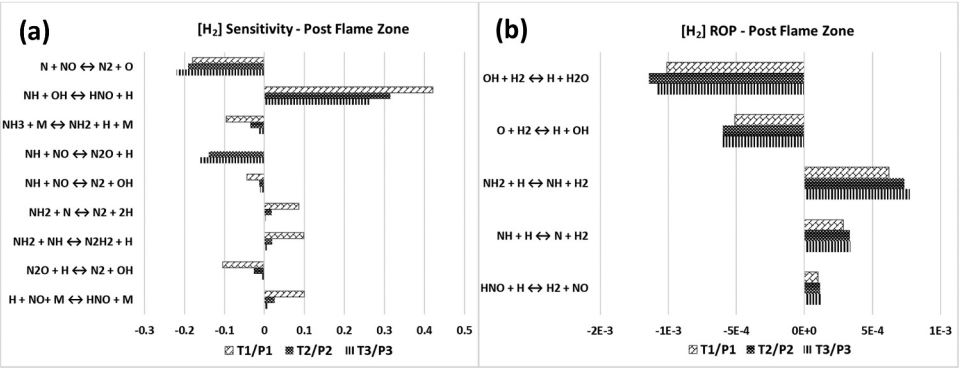

Figure 21. (a) Normalized sensitivity coefficients, and (b) absolute ROP of [H_2] at the post flame zone.

forward direction for T1/P1 condition whilst showing backward trends for T2/P2 and T3/P3 conditions, resulting in opposing sensitivity for overall NH_2 at the post-flame zone.

Figure 19a,b, illustrates the absolute ROP of NH_3 at the flame zone and the post-flame zone, respectively. Rate of consumption and production of NH_3 is about 4 times higher at the post-flame zone than the flame zone due to the rich combustion condition. NH_3 converts to NH_2 by reacting with H and OH radicals and NH_2 converts back to NH_3 through reaction R2 operating backwards at both flame and post-flame zones. Additionally, small amounts of NH_3 react with O radicals to produce NH_2 radicals and NH_2 radicals convert back to NH_3 through decomposition/addition reaction $2NH_2 \leftrightarrow NH_3 + NH$ (R7) at the flame zone.

Next, sensitivity analysis was carried out for H_2, which is an important part of the fuel blend under consideration. Computed normalized sensitivity coefficients of H_2 at flame zone and post-flame zone are displayed in Figures 20a and 21a, respectively. Due to the rich combustion condition, reaction R1 only shows sensitivity to H_2 at the flame zone where all the relevant intermediate species (i.e. H, O and OH) are formed and play an important role to oxidize the fuel and reduce ignition delay time (Mashruk, Xiao, Valera-Medina 2020; Warnatz, Maas, Dibble 2006). Other than reaction R1, all the other reactions responsible for H_2 concentrations at the flame zone (Figure 20a) show opposite effect to NH_2 concentrations (Figure 17a) at the flame zone for all the inlet conditions under consideration. H_2 reacts with OH and O radicals to produce H radicals, which in turn decomposes nitrogen-based species NH_3, NH_2, NH, N_2H_2 etc. to enhance ammonia reactivity, Figure 20b. Reactions responsible for H_2 sensitivity at the post-flame zone, Figure 21a, feature quite a few reactions involving NO and N_2O. These reactions have highest sensitivity at T1/P1 condition, thus giving lowest NO readings both experimentally and numerically at this condition. These reactions will be discussed further at the following part of the analysis. Similar reactions feature at the post-flame zone for overall H_2 concentration, Figure 21b, as at the flame zone but with considerably higher ROP values.

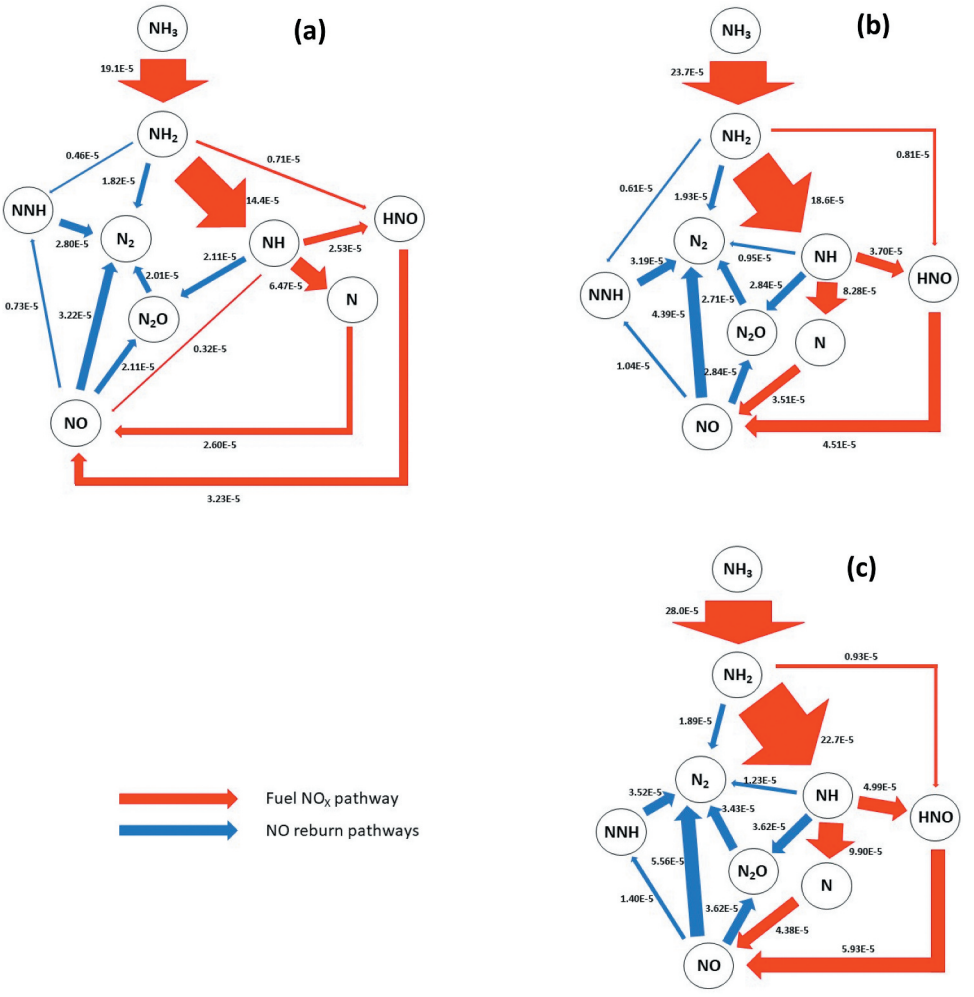

Figure 22. Quantitative reaction path diagram showing NO formation/reburn pathways at the flame zone for (a) T1/P1, (b) T2/P2, and (c) T3/P3 conditions.

Finally, NO sensitivity analysis has been conducted to identify the reactions responsible for NO formation and consumption with changing inlet conditions. Initially, NO formation/consumption at the flame zone is analyzed with aids of quantitative reaction path diagrams (QRPD), Figure 22, and normalized sensitivity coefficients of NO, Figure 23. As described earlier, NH_3 converts to NH_2 by reacting with H and OH radicals. NH_2 then primarily convert to NH by reacting further with H and OH radicals. NH_2 also converts to molecular N_2 and nitric acid by reacting with atomic N and O radicals, respectively. NH radicals then react with OH to produce HNO and H radicals. This particular reaction is the major source of HNO production, thus having the highest positive sensitivity of NO, Figure 23a. Remaining NH radicals convert to atomic N and molecular H_2 through the reaction NH + H ↔ N + H_2 (R8). HNO then produce NO through the reactions HNO + H ↔ H_2 + NO (R9) and H + NO + M ↔ HNO + M (R10), operating backwards. Atomic

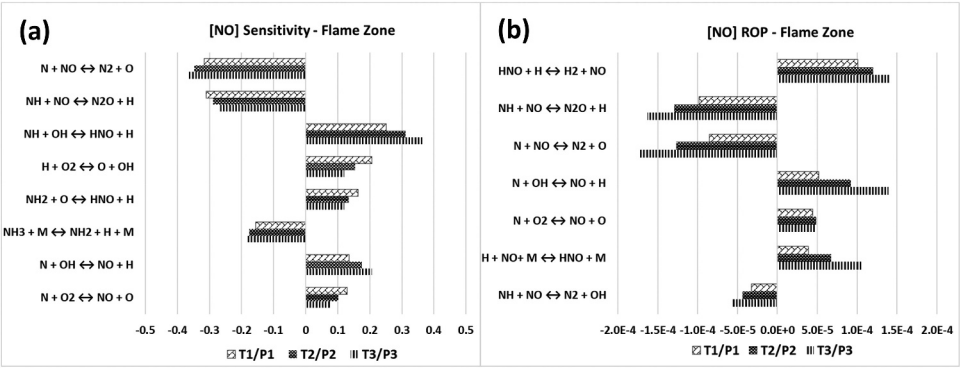

Figure 23. (a) Normalized sensitivity coefficients, and (b) absolute ROP of [NO] at the flame zone.

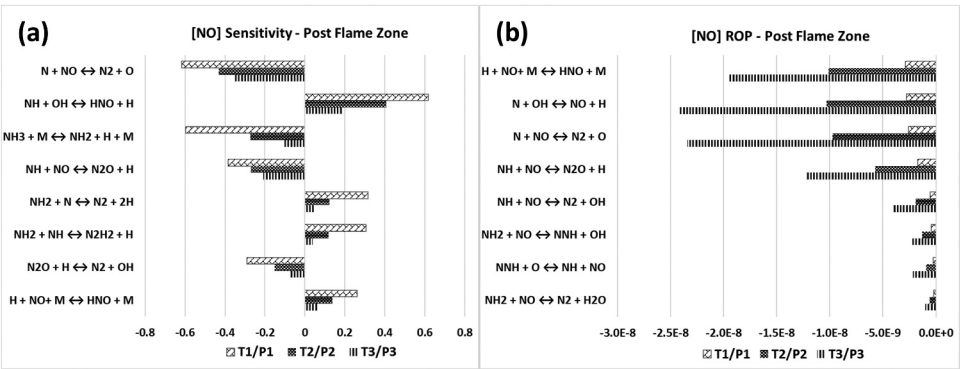

Figure 24. (a) Normalized sensitivity coefficients, and (b) absolute ROP of [NO] at the post flame zone.

N reacts with OH through the reaction N + OH ↔ NO + H (R11) and molecular O_2 to produce further NO. Interestingly, the proportion of NO production from N reacting with O_2 compared to OH radicals decrease as inlet conditions elevates to higher T/P, Figure 23a.

NO formed in the flame zone mostly converts to N_2 by reacting with atomic N, NH and NH_2 radicals in decreasing order, reflecting in high negative NO sensitivity. Some of the NO also convert to N_2 via NNH. Some N_2O is also formed from NO through the reaction NH + NO ↔ N_2O + H (R12). This reaction has second highest negative sensitivity for NO concentration at the flame zone after N + NO ↔ N_2 + O (R13). Most of the nitrous oxide produced in the flame zone convert to N_2 by reacting with atomic H and through the third body reaction N_2O (+M) ↔ N_2 + O (+M) (R14).

Figure 24 details the computed normalized sensitivity and absolute ROP of NO concentration at the post-flame zone. Most of the NO produced at the flame zone burns away at the post-flame zone. Contrary to the flame zone, reactions R10 and R11 operate at opposite direction to contribute toward NO consumption at the post-flame zone for all the inlet conditions. Significant amount of NO also convert directly to N_2 through reaction R13 and via N_2O through reactions R12 and R14. Reaction rates for NO

consumption at the post-flame zone are four orders of magnitude lower than flame zone and increases considerably for the elevated conditions compared to T1/P1 condition at post-flame zone.

Overall, an increasing trend in the reaction rates was observed with increasing inlet conditions, even though the inlet flow rates were kept constant for this study, an expected result. NH_x radicals were shown to be produced in the flame zone through the reactions between NH_3 and H, O and OH radical pools. Presence of H_2 in the fuel blend was shown to increase reactivity of ammonia via increased production of these radicals. However, the production of NO at the flame zone was highly dependent of NH_2 radicals via HNO and atomic N. However, most of the NO produced at the flame zone shown to be consumed at the post-flame zone due to the presence of atomic N and NH_x radicals.

Conclusions

Fully premixed $70/30_{vol\%}$ NH_3/H_2 swirl flames were investigated numerically in Chemkin-Pro and Star-CCM+ environments to evaluate the changes in NH_2 formation at three different T/P conditions with an equivalence ratio of 1.2 and its effect on NO concentration. CFD calculations were validated for isothermal conditions in terms of hydrodynamics of the system with the aid of LDA measurements and with emissions from experimental tests for combustion conditions. Okafor's mechanism was employed for this investigation due to its low computational costs and similar prediction trends with experimental data. In addition, detailed sensitivity and ROP analysis were carried out to understand and identify the reaction pathways involved in the formation and consumption of NO under different conditions. The main conclusions of this study are summarized as follows.

(1) NH_2 production peaks correlated with highest chemical heat release, as well as other important species like O, NH and NNH, while negative correlation was demonstrated for NH_3, with hints of some negative correlation with H_2 and N_2 H_3. NO and N_2O production peaks were captured near NH_2 peaks at the flame front, showing a direct link of NH_2 radicals to their production. However, NO_2 was found to be mostly consumed within these NH_2 peaks, mainly due to the high NH_2 concentration and presence of high temperature. This led to decomposition and recombination of N_2O in the flame. NO reburn was found to be correlated with the consumption of NNH, O, NH_2 radicals and increase in residence time.
(2) At higher inlet temperatures and pressures, NH_2 production/consumption rate increases due to contracted flame zone, resulting in thinner, more active reaction layer and increased NO production. NO produced at the flame zone was mostly consumed at the post-flame zone due to the higher availability of NH_2 radicals and unburned ammonia.
(3) The Q-criterion was employed to identify correlation between vorticity and NH_2 production. Vortices were located near the dumping plane and through the boundaries of the flame and recirculation zone but NH_2 was only found to be produced at the upper vortical structures with the turbulence model used in this investigation.

Hence, further analyses are recommended with more detailed turbulence models to elucidate the impact of vortical structures, which seems to occur within the inner part of the flame.

(4) Sensitivity and ROP analysis for NH_2, H_2 and NO further validated these findings. The reactions $NH_3 + OH \leftrightarrow NH_2 + H_2O$ and $NH_2 + H \leftrightarrow NH + H_2$ were shown to have maximum sensitivity for NH_2 production and consumption, respectively, irrespective of inlet conditions and combustion locations. H_2 sensitivity analysis showed opposite sensitivity to NH_2 for the same reactions as H_2 plays an important role to enhance NH_3 flammability by forming H, O and OH radicals.

(5) Atomic nitrogen was found to be main contributor toward NO reduction to molecular nitrogen and the largest source of NO production was NH radicals forming through $NH_3 \rightarrow NH_2 \rightarrow NH$ pathway, which reacts to OH radicals to form HNO and then NO. The branching ratio of the NO reburn reactions $NH + NO \leftrightarrow N_2O + H$ and $NH + NO \leftrightarrow N_2 + OH$ are critical to contain the greenhouse gas N_2O, and further studies are recommended here.

Acknowledgments

The authors gratefully acknowledge the support from EPSRC through the project SAFE-AGT Pilot (no. EP/T009314/1). Information on the data underpinning the results presented here, including how to access them, can be found in the Cardiff University data catalogue at http://orca.cf.ac.uk/144278.

Disclosure statement

No potential conflict of interest was reported by the author(s).

Funding

This work was supported by the Engineering and Physical Sciences Research Council [SAFE-AGT Pilot (no. EP/T009314/1)].

ORCID

Syed Mashruk http://orcid.org/0000-0002-3049-4932
Meng-Choung Chiong http://orcid.org/0000-0002-1815-3887
Agustin Valera-Medina http://orcid.org/0000-0003-1580-7133

References

Baej, H., A. Valera-Medina, P. Bowen, N. Syred, T. O'Doherty, and R. Marsh. 2014. Impacts on blowoff by a variety of CRZs using various gases for gas turbines. *Energy Procedia* 61:1606–09. doi:10.1016/j.egypro.2014.12.301.

British Standard. 1996. *BS ISO 11042-1:1996. Gas turbines-exhaust gas emission.*

Colson, S., Y. Hirano, A. Hayakawa, T. Kudo, H. Kobayashi, C. Galizzi, and D. Escudié. 2020. Experimental and numerical study of NH3/CH4 counterflow premixed and non-premixed flames for various NH3 mixing ratios. *Combust. Sci. Technol.* 1–18. doi:10.1080/00102202.2020.1763326.

Comotti, M., and S. Frigo. 2015. Hydrogen generation system for ammonia-hydrogen fuelled internal combustion engines. *Int. J. Hydrogen Energy* 40 (33):10673–86. doi:10.1016/j.ijhydene.2015.06.080.

Coutant, R. W., E. L. Merryman, and A. Levy. 1982. Formation of NO2 in range-top burners. *Environ. Int.* 8 (1–6):185–92. http://files/245/0160412082900277.html .

Dantec Dynamics. 2017. *BSA flow software for LDA*.

Elishav, O., B. Mosevitzky Lis, E. M. Miller, D. J. Arent, A. Valera-Medina, A. Grinberg Dana, G. E. Shter, and G. S. Grader. 2020. Progress and prospective of nitrogen-based alternative fuels. *Chem. Rev.* 120 (12):5352–436. doi:10.1021/acs.chemrev.9b00538.

Eriksson, P. 2007. The zimont TFC model applied to premixed bluff body stabilized combustion using four different rans turbulence models. *Proc. ASME Turbo Expo.* 2:353–61. doi:10.1115/GT2007-27480.

Ezzat, M. F., and I. Dincer. 2018. Comparative assessments of two integrated systems with/without fuel cells utilizing liquefied ammonia as a fuel for vehicular applications. *Int. J. Hydrogen Energy* 43 (9):4597–608. doi:10.1016/j.ijhydene.2017.07.203.

Glarborg, P., J. A. Miller, B. Ruscic, and S. J. Klippenstein. 2018. Modeling nitrogen chemistry in combustion. In *Progress in energy and combustion science*, Vol. 67, 31–68. Elsevier Ltd. doi:10.1016/j.pecs.2018.01.002.

Gordon, S., and B. J. McBride. 1976. Computer program for calculation of complex chemical equilibrium compositions rocket performance incident and reflected shocks, and Chapman-Jouguet detonations. In *NASA reference publication*, 1311.

Guteša Božo, M., S. Mashruk, S. Zitouni, and A. Valera-Medina. 2021. Humidified ammonia/hydrogen RQL combustion in a trigeneration gas turbine cycle. *Energy Convers. Manage.* 227:113625. doi:10.1016/j.enconman.2020.113625.

Hayakawa, A., T. Goto, R. Mimoto, T. Kudo, and H. Kobayashi. 2015. NO formation/reduction mechanisms of ammonia/air premixed flames at various equivalence ratios and pressures. *Mech. Eng. J.* 2 (1):14-00402-14–00402. doi:10.1299/mej.14-00402.

International Energy Agency. 2019. *The future of hydrogen - executive report*.

Jeong, J., and F. Hussain. 1995. On the identification of a vortex. *J. Fluid Mech.* 285:69–94. doi:10.1017/S0022112095000462.

Jolliffe, I. T., and J. Cadima. 2016. Principal component analysis: A review and recent developments. *Philos. Trans. R. Soc. A.* 374:2065. doi:10.1098/RSTA.2015.0202.

Jolliffe, I. T. 2002. *Principal component analysis*. 2nd ed. Springer-Verlag. doi:10.1007/B98835. Springer, New York, NY.

Kee, R. J., J. F. Grcar, M. D. Smooke, J. A. Miller, and E. Meeks. 1985. PREMIX: A Fortran program for modeling steady laminar one-dimensional premixed flames. *Sandia National Laboratories Report, SAND85-8249*. http://www.scc.acad.bg/ncsa/articles/library/Library2014_Supercomputers-at-Work/Computational_FluidDynamics/PREMIXcodeSandia.pdf

Khateeb, A. A., T. F. Guiberti, X. Zhu, M. Younes, A. Jamal, and W. L. Roberts. 2020. Stability limits and NO emissions of technically-premixed ammonia-hydrogen-nitrogen-air swirl flames. *Int. J. Hydrogen Energy* 45 (41):22008–18. doi:10.1016/j.ijhydene.2020.05.236.

Klippenstein, S. J., L. B. Harding, P. Glarborg, and J. A. Miller. 2011. The role of NNH in NO formation and control. *Combust. Flame* 158 (4):774–89. doi:10.1016/j.combustflame.2010.12.013.

Kobayashi, H., A. Hayakawa, K. D. K. A. Somarathne, and E. C. Okafor. 2018. Science and technology of ammonia combustion. *Proc. Combust. Inst.* doi:10.1016/j.proci.2018.09.029.

Kobayashi, H., A. Hayakawa, K. D. K. A. Somarathne, and E. C. Okafor. 2019. Science and technology of ammonia combustion. *Proc. Combust. Inst.* 37 (1):109–33. doi:10.1016/j.proci.2018.09.029.

Konnov, A. A. 2009. Implementation of the NCN pathway of prompt-NO formation in the detailed reaction mechanism. *Combust. Flame* 156 (11):2093–105. doi:10.1016/j.combustflame.2009.03.016.

Kurata, O., N. Iki, T. Inoue, T. Matsunuma, T. Tsujimura, H. Furutani, M. Kawano, K. Arai, E. C. Okafor, A. Hayakawa, et al. 2019. Development of a wide range-operable, rich-lean low-NOx combustor for NH 3 fuel gas-turbine power generation. *Proc. Combust. Inst.* 37:4587–95. doi:10.1016/j.proci.2018.09.012.

Lhuillier, C., P. Brequigny, F. Contino, and C. Rousselle. 2019. Performance and emissions of an ammonia-fueled SI engine with hydrogen enrichment. *SAE Technical Papers, 2019-Septe* (September). doi:10.4271/2019-24-0137.

Li, R., G. He, F. Qin, C. Pichler, and A. A. Konnov. 2019a. Comparative analysis of detailed and reduced kinetic models for CH4 + H2 combustion. *Fuel*. doi:10.1016/j.fuel.2019.02.132.

Li, R., A. A. Konnov, G. He, F. Qin, and D. Zhang. 2019b. Chemical mechanism development and reduction for combustion of NH3/H2/CH4 mixtures. *Fuel*. doi:10.1016/j.fuel.2019.116059.

Lindstedt, R. P., F. C. Lockwood, and M. A. Selim. 1994. Detailed kinetic modelling of chemistry and temperature effects on ammonia oxidation. *Combust. Sci. Technol.* 99 (4–6):253–76. doi:10.1080/00102209408935436.

Manna, M., P. Sabia, R. Ragucci, and M. de Joannon. 2019. Experimental study of ammonia oxidation in a jet stirred flow reactor: Data consistency with kinetic mechanism results and wall effects. *14th International Conference on Energy for a Clean Environment,*Funchal, Madeira, Portugal.

Mashruk, S., H. Xiao, and A. Valera-Medina. 2020. Rich-Quench-Lean model comparison for the clean use of humidified ammonia/hydrogen combustion systems. *Int. J. Hydrogen Energy* 46 (5):4472–84. doi:10.1016/j.ijhydene.2020.10.204.

Mashruk, S. 2020. NO formation analysis using chemical reactor modelling and LIF measurements on industrial swirl Flames. PhD Thesis, Cardiff University. https://doi.org/10.13140/RG.2.2.28297.06246/1

Mathieu, O., and E. L. Petersen. 2015. Experimental and modeling study on the high-temperature oxidation of ammonia and related NOx chemistry. *Combust. Flame* 162 (3):554–70. doi:10.1016/j.combustflame.2014.08.022.

Miller, J. A., and C. T. Bowman. 1989. Mechanism and modeling of nitrogen chemistry in combustion. *Prog. Energy Combust. Sci.* 15:287–338. doi:10.1016/0010-2180(91)90047-F.

Miller, J. A., M. C. Branch, W. J. Mclean, D. W. Chandler, M. D. Smooke, and R. J. Kee. 1985. The conversion of HCN to NO and N2 in H2- O2- HCN- Ar flames at low pressure. 20: 673–84. http://files/241/S0082078485805579.html

Okafor, E. C., Y. Naito, S. Colson, A. Ichikawa, T. Kudo, A. Hayakawa, and H. Kobayashi. 2018. Experimental and numerical study of the laminar burning velocity of CH4–NH3–air premixed flames. *Combust. Flame* 187:185–98. doi:10.1016/j.combustflame.2017.09.002.

Pacheco, G. P., R. C. Rocha, M. C. Franco, M. A. A. Mendes, E. C. Fernandes, P. J. Coelho, and X. S. Bai. 2021. Experimental and kinetic investigation of stoichiometric to rich NH3/H2/Air flames in a swirl and bluff-body stabilized burner. *Energy Fuels* 35 (9):7201–16. doi:10.1021/acs.energyfuels.0c03872.

Pearse, R. W., and A. G. Gaydon. 1976. The identification of molecular spectra. In *Chapman and Hall.* 4th ed., ed. B. P. Straughan and S. Walker. Springer Netherlands.

Prada, L., and J. A. Miller. 1998. Reburning using several hydrocarbon fuels: A kinetic modeling study. *Combust. Sci. Technol.* 132 (1–6):225–50. http://files/233/andMiller-1998-Reburningusingseveralhydrocarbonfuelsakinet.pdfPrada .

Pugh, D., P. Bowen, A. Valera-Medina, A. Giles, J. Runyon, and R. Marsh. 2019. Influence of steam addition and elevated ambient conditions on NOx reduction in a staged premixed swirling NH3/H2 flame. *Proc. Combust. Inst.* 37 (4):5401–09. doi:10.1016/j.proci.2018.07.091.

Pugh, D., J. Runyon, P. Bowen, A. Giles, A. Valera-Medina, R. Marsh, B. Goktepe, and S. Hewlett. 2020. An investigation of ammonia primary flame combustor concepts for emissions reduction with OH*, NH2* and NH* chemiluminescence at elevated conditions. *Proc. Combust. Inst.* doi:10.1016/j.proci.2020.06.310.

Rocha, R. C., C. F. Ramos, M. Costa, and X. S. Bai. 2019. Combustion of NH3/CH4/Air and NH3/H2/air mixtures in a porous burner: Experiments and kinetic modeling. *Energy Fuels* 33 (12):12767–80. doi:10.1021/acs.energyfuels.9b02948.

The Royal Society. 2020. *Ammonia: Zero-carbon fertiliser, fuel and energy store*. royalsociety.org/green-ammonia.

Runyon, J., R. Marsh, P. Bowen, D. Pugh, A. Giles, and S. Morris. 2018. Lean methane flame stability in a premixed generic swirl burner: Isothermal flow and atmospheric combustion characterization. *Exp. Therm. Fluid Sci.* 92:125–40. doi:10.1016/j.expthermflusci.2017.11.019.

Runyon, J., R. Marsh, A. Valera-Medina, A. Giles, S. Morris, D. Pugh, Y. Sevcenco, and P. Bowen. 2015. Methane-oxygen flame stability in a generic premixed gas turbine swirl combustor at varying thermal power and pressure. *Proc. ASME Turbo Expo.* 4B. doi:10.1115/GT201543588.

Siemens. 2019. *Complex chemistry*. Star-CCM+ Documentation.

Skreiberg, Ø., P. Kilpinen, and P. Glarborg. 2004. Ammonia chemistry below 1400 K under fuel-rich conditions in a flow reactor. *Combust. Flame* 136 (4):501–18. doi:10.1016/j.combustflame.2003.12.008.

Tian, Z., Y. Li, L. Zhang, P. Glarborg, and F. Qi. 2009. An experimental and kinetic modeling study of premixed NH3/CH4/O2/Ar flames at low pressure. *Combust. Flame* 156 (7):1413–26. doi:10.1016/j.combustflame.2009.03.005.

Valera-Medina, A. 2020. Ammonia gas turbines. *ETN Annual General Meeting and Workshop*, 59.

Valera-Medina, A., F. Amer-Hatem, A. K. Azad, I. C. Dedoussi, M. de Joannon, R. X. Fernandes, P. Glarborg, H. Hashemi, X. He, S. Mashruk, et al. 2021. Review on ammonia as a potential fuel: From synthesis to economics. *Energy Fuels* 35 (9):6964–7029. doi:10.1021/acs.energyfuels.0c03685.

Valera-Medina, A., M. Gutesa, H. Xiao, D. Pugh, A. Giles, B. Goktepe, R. Marsh, and P. Bowen. 2019. Premixed ammonia/hydrogen swirl combustion under rich fuel conditions for gas turbines operation. *Int. J. Hydrogen Energy* 44 (16):8615–26. doi:10.1016/j.ijhydene.2019.02.041.

Valera-Medina, A., M. Gutesa, H. Xiao, D. Pugh, A. Giles, B. Goktepe, R. Marsh, and P. J. Bowen. 2018a. Premixed ammonia/hydrogen swirl combustion under fuel-rich conditions for gas turbines operation. *Proc. Combust. Inst. Under Revi* (16):8615–26. doi:10.1016/j.ijhydene.2019.02.041.

Valera-Medina, A., R. Marsh, J. Runyon, D. Pugh, P. Beasley, T. Hughes, and P. Bowen. 2017. Ammonia–methane combustion in tangential swirl burners for gas turbine power generation. *Appl. Energy* 185:1362–71. doi:10.1016/j.apenergy.2016.02.073.

Valera-Medina, A., N. Syred, and P. Bowen. 2013. Central recirculation zone visualization in confined swirl combustors for terrestrial energy. *J. Propul. Power* 29:1. doi:10.2514/1.B34600.

Valera-Medina, A., H. Xiao, M. Owen-Jones, W. I. F. David, and P. J. Bowen. 2018b. Ammonia for power. *Prog. Energy Combust. Sci.* 69:63–102. doi:10.1016/j.pecs.2018.07.001.

Valera-Medina, A., A. Giles, D. Pugh, S. Morris, M. Pohl, and A. Ortwein. 2018c. Investigation of combustion of emulated biogas in a gas turbine test rig. *J. Therm. Sci.* 27 (4):331–40. doi:10.1007/s11630-018-1024-1.

Vigueras-Zuniga, M., M. Tejeda-del-Cueto, J. Vasquez-Santacruz, A. Herrera-May, and A. Valera-Medina. 2020. Numerical predictions of a swirl combustor using complex chemistry fueled with ammonia/hydrogen blends. *Energies* 13 (2):288. doi:10.3390/en13020288.

Warnatz, J., U. Maas, and R. W. Dibble. 2006. *Combustion: Physical and chemical fundamentals, modeling and simulation, experiments, pollutant formation*. 4th ed. Springer-Verlag. https://www.springer.com/gp/book/9783540259923 .

Zamfirescu, C., and I. Dincer. 2008. Using ammonia as a sustainable fuel. *J. Power Sources* 185:459–65. doi:10.1016/j.jpowsour.2008.02.097.

Zhu, X., A. A. Khateeb, T. F. Guiberti, and W. L. Roberts. 2021. NO and OH* emission characteristics of very-lean to stoichiometric ammonia–hydrogen–air swirl flames. *Proc. Combust. Inst.* 38 (4):5155–62. doi:10.1016/j.proci.2020.06.275.